Journal of the Serbian Chemical Society
JSCS@tmf.bg.ac.rs • www.shd.org.rs/JSCS

J. Serb. Chem. Soc. *87* (5) 545–559 (2022)
JSCS–5540

Original scientific paper
Published 18 February 2022

Structural, biological and computational study of oxamide derivative

IGNJAT P. FILIPOVIĆ[1#], EMINA M. MRKALIĆ[2], GIORGIO PELOSI[3], VESNA KOJIĆ[4], DIMITAR JAKIMOV[4], DEJAN BASKIĆ[5] and ZORAN D. MATOVIĆ[1]*

[1]*University of Kragujevac, Faculty of Science, Department of Chemistry, Radoja Domanovića 12, 34000 Kragujevac, Serbia,* [2]*University of Kragujevac, Institute for Information Technologies, Department of Science, Jovana Cvijića bb, Kragujevac 34000, Serbia,* [3]*Department of Chemistry, Life Sciences and Environmental Sustainability, University of Parma, 43123 Parma, Italy,* [4]*Institute of Oncology Sremska Kamenica, Novi Sad, Institutski put 4, 21204 Sremska Kamenica, Serbia and* [5]*University of Kragujevac, Faculty of Medicinal Science, S. Markovića 69, 34000 Kragujevac, Serbia*

(Received 4 December, revised 28 December, accepted 29 December 2021)

Abstract: A dicarboxylato-diamide-type compound 2,2'-[(1,2-dioxoethane-1,2--diyl)diimino]dibenzoic acid (H_4obbz) (**1**) was synthesized and characterized. The crystal structure of K_2H_2obbz·$2H_2O$ (**2**) was determined by X-ray diffraction analysis. The cytotoxic activities of the compounds were tested against four different cancer cell lines MCF-7, A549, HT-29, HeLa and a human normal cell line MRC-5. The results indicate reasonable dose-dependent cytotoxicity of the ligands that show selectivity against the tested carcinoma and healthy cell lines. Flow cytometric analysis and fluorescence microscopy showed that the most active compound, H_4obbz, induced apoptosis and G0/G1 cell cycle arrest, indicating blockage of DNA synthesis as a possible mechanism that triggers apoptosis. Docking and molecular dynamics simulations gave similar responses regarding interactions (binding) between their ligands and chaperon Grp78. The MMGBSA determined ΔG binding energies were in the range from –104 to –140 kJ mol^{-1}.

Keywords: oxamides; crystal structure; apoptosis; docking; molecular dynamics.

INTRODUCTION

Very recently, a mechanism of the drug action adopting interactions of heat shock proteins (HSP) chaperons was proposed. The IC_{50} value of the tested compound appears to be comparable with those of commercial drugs that are in clin-

* Corresponding author. E-mail: zmatovic@kg.ac.rs
# Serbian Chemical Society member.
https://doi.org/10.2298/JSC211204114F

ical use.[1,2] Between the chosen macromolecules to which the compounds were computationally simulated, the group of chaperon proteins (Grp78 from endoplasmic reticulum (ER) and Hsc70 from cytosol) were evidenced as better hosts than oligonucleotides (DNA). Furthermore, it was found that the different substituents on oxamide nitrogens resulted in the difference in cytotoxicity of the compounds. Interactions of anthranilic acid oxamidate-derivative with the membrane layer, membrane protein channels and components within cytosol (DNA, peptides/proteins) were much more suitable than that of other derivatives. Antiproliferative activity of the drug may also result from its cytostatic (effect on cell cycle) or cytotoxic effects (*e.g.*, apoptosis induction). The anti-apoptotic protein Bcl-2 plays a key role in apoptosis. Its suppressive activity in the apoptotic process may contribute to the drug resistance of tumor cells.[3–6] Intermolecular interactions, and modes of binding in the active site of an enzyme, can be determined by molecular docking. For example, targeting Grp78, and comparing binding modes of ATP and potential inhibitor can provide important insights about the cytotoxicity of a compound towards both cancerous and healthy cells.[7] At the same time, a molecular dynamics (MD) study may give an answer about the conformational and energetic change of the *holo*-protein during the time of the production run. In this paper, how the addition of an aromatic group on the arm chains of an oxamide might improve their biological activity is reported. Also, qualitative and quantitative tests on treated cells using techniques such as flow-cytometry and western-blot analysis are reported. Quantum mechanics, docking, and MD were used to further support the biological results on the interaction of the compound with malignant cells.

EXPERIMENTAL

Materials and measurements

All other chemicals of analytical reagent grade were commercially purchased and used without further purification. Elemental microanalyses for C, H, N were performed at the Microanalytical Laboratory, Faculty of Chemistry, University of Belgrade, Serbia. IR spectra were obtained in KBr pellets using a Perkin–Elmer FT-IR Spectrum One spectrophotometer. The positions of the absorbance bands are expressed in cm^{-1} and the intensities are labelled as *w* (weak), *m* (medium) or *s* (strong). Only the most significant absorption bands are reported. ^{1}H- and ^{13}C-NMR spectra were recorded on a Varian Gemini 2000 spectrometer (200 MHz). Chemical shifts are expressed as δ values (ppm) relative to 3-trimethylsilylpropionic acid-*d*4 sodium salt (TSP) as internal standard. Coupling constants *J* are given in Hz. Melting points were determined using Stuart digital melting point apparatus with accuracy ± 1 °C. The chemicals and solvents used were commercially available.

Analytical and spectral data are given in Supplementary material to this paper.

*Synthesis of 2,2'-[(1,2-dioxoethane-1,2-diyl)diimino] dibenzoic acid, H_4obbz (**1**)*[8]

To a stirred solution of anthranilic acid (3.0 g, 2.2×10^{-2} mol) in THF (50 mL) was added dropwise a solution of oxalyl chloride (1.3 g, 10^{-2} mol). The solution was stirred for 1 h. The

acid that precipitated as a white powder was filtered off under vacuum, washed with THF and air-dried. Yield: 2.50 g (74.40 %).

*Synthesis of $K_2H_2obbz·2H_2O$ (**2**)*

To a stirred solution of H_4obbz (**1**, 0.328 g, 1×10^{-3} mol) a solution of potassium hydroxide (0.112 g, 2×10^{-3} mol) was added dropwise. The solution was left in a refrigerator for a few days. The formed crystals were isolated. Yield: 0.26 g (59.6 %).

X-Ray structure determinations

Suitable crystals of **2** were grown by slow evaporation from a water solution at room temperature. X-ray diffraction data were collected using a SMART APEX diffractometer equipped with CCD detector, MoKα radiation (λ = 0.71069 Å) and corrected for absorption effects following the SADABS[9] procedure. The phase problem was solved by direct methods and the structures were refined by full-matrix least-squares on all F^2 using SHELXL97[10], as implemented in WINGX.[11] Analytical expressions of the scattering factors of neutral atoms were taken from the International Tables for X-Ray Crystallography.[12] The structure drawing was obtained using ORTEPIII.[13] Data are given in Table I.

TABLE I. Crystal structure and refinement data for compound **2**

Compound reference	K_2H_2obbz	Temperature, K	293(2)
Chemical formula	$C_8H_5KNO_4$	Space group	$R\bar{3}$
Formula Mass	218.23	No. of formula units per unit cell	18
Crystal system	Trigonal	No. of reflections measured	10544
a / Å	28.145(4)	No. of independent reflections	2281
b / Å	28.145(4)	R_{int}	0.0898
c / Å	6.484(1)	Final R_1 ($I > 2\sigma(I)$)	0.0781
α / °	90.00	Final wRF^2 ($I > 2\sigma(I)$)	0.2312
β / °	90.00	Final R_1 (all data)	0.1740
γ / °	120.00	Final wRF^2 (all data)	0.3043
Unit cell volume, Å^3	4448(2)	CCDC number	1412205

Quantum-mechanical method

Density functional theory (DFT) calculations were performed by the Gaussian 09 suite.[14] The Becke three-parameter exchange functional, in conjunction with the Lee-Yang-Parr correlation functional (B3LYP),[15-17] with the Ahlrich triple valence basis set (TZVP)[18] was used. All calculated structures were verified to be local minima (all positive eigenvalues) for ground state structures.

Docking method

Molecular docking of ligands (ATP, H_2obbz^{2-} and H_4obbz) was simulated to the three-dimensional X-ray structure of Grp78 (ref. code 3LDL[19]). This protein is Hsc70 isoform and originates from ER.[19] Docking processes were performed using AutoDock 4.2 (AD4)[20] and AutoDock Vina (Vina)[21] software equipped with a graphical user interface (GUI) AutoDock Tools 1.5.6rc3 (ADT). Full description of the methods used can be found in the Supplementary material.

MM/MD simulations

The Amber20 program[22] was used to parametrize protein complexes. The ff19SB force field, [22] TIP4P OPC water model,[23,24] and Na^+ and Cl^- parameters from Li *et al.*[25] were used

to model the protein monomer, water molecules in the solvation box, and Na^+ and Cl^-, respectively. Grp78 monomer was obtained from 3LDL X-ray PDB structure. For parametrization, ATP, H_2obbz^{2-} and H_4obbz were taken from DFT optimized structures. The best scored docking structures were used for the simulation runs. AmberTools21[22] was used for the structural modeling and data analyses while pmemd.cuda[26-28] in AMBER20[22] was employed in the MD simulation. The three ligands and corresponding Grp78-[L] complexes were modeled, simulated (MM/MM regime) and ΔG (MMGBSA method) determined in the way as described in detail in the Supplementary material.

Cell lines

The cell lines used in the study were MCF-7 (human breast adenocarcinoma), A549 (human lung carcinoma), HT-29 (human colon adenocarcinoma), HeLa (human cervix adenocarcinoma) and MRC-5 (human fetal lung fibroblasts). The cells were grown in Dulbecco's modified Eagle's medium (DMEM) with 4.5 % of glucose, supplemented with 10 % of fetal bovine serum (FBS, Sigma) and antibiotics and antimicotics solution (Sigma). All cell lines were cultivated at 37 °C in an atmosphere of 5 % CO_2 and absolute humidity.

Assays and analysis

Details for MTT assay, Annexin V-FITC/7-AAD assay for determination of apoptosis and necrosis by flow cytometry, Western blot analysis, and Cell cycle Analysis by flow cytometry are given in the cited works[29-31] and in the Supplementary material.

RESULTS AND DISCUSSION

Preparative work and spectral analysis

The syntheses of H_4obbz (**1**) and K_2obbz (**2**) are outlined in Scheme 1.

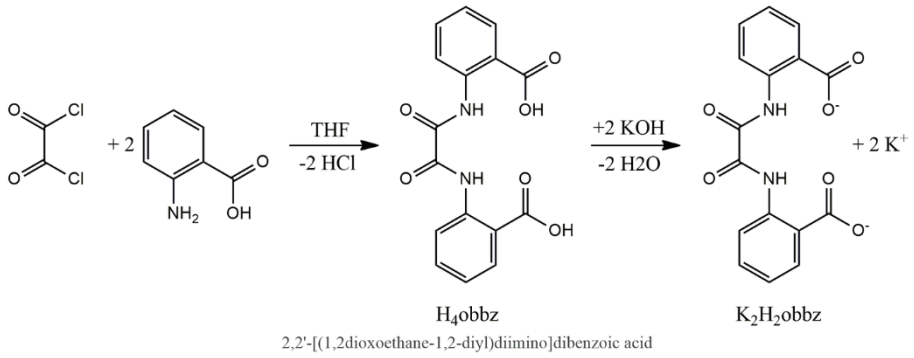

Scheme 1. Preparative path of compounds **1** and **2**.

Infrared spectra of the ligands show the characteristic absorptions of the corresponding amido-carboxylate groups, a strong and sharp ν(NH) and ν(COOH) vibration in the range observed for the compounds (**1**: 3268, 1701 cm^{-1}, **2**: 3322, 1712 cm^{-1}, Fig. S-4 of the Supplementary material). The ^1H- and ^{13}C-NMR spectra of the investigated compounds were recorded. The ^{13}C-NMR spectra showed all the carbon signals on the expected position, which further provides

support for their structures. The ^{1}H-NMR spectraum of the compound **1** consists of phenyl group signals in the δ range 6.2–8.4 ppm.

Structure

The molecular structure and crystal packing of compound **2** $K_2H_2obbz{\cdot}2H_2O$, are depicted in Fig. 1. The coordination sphere of potassium in **2** is shown in Fig. S-5 of the Supplementary material.

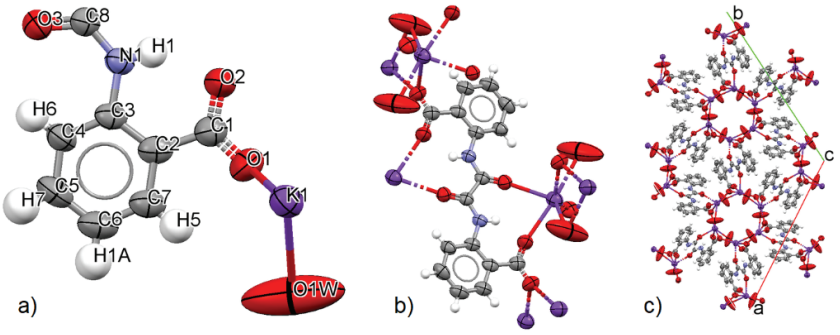

Fig. 1. Ortep diagram of $K_2H_2obbz{\cdot}2H_2O$ (**2**) structure: a) asymmetric unit with labeled atoms; b) molecular structure; c) crystal packing view along the *c* axis.

Selected bond lengths and bond angles for this compound are gathered in Table II (complete data are in Tables S-II–S-IV of the Supplementary material). Compound **2** crystallized as a dipotassium salt of compound **1**, in which the potassium ion coordinated to the carboxylic oxygen atom O2 and the amide oxygen O3 atom. This compound crystallizes as the more stable *trans* conformer in the trigonal crystal system with $R\bar{3}$ space group. The independent asymmetric unit of **2** comprises a half molecule of the anionic ligand of Cs symmetry. The asymmetric units associated with potassium atoms and water molecules form hexagonal cavities. Bonds C8−O3 and C8−N1 have lengths typical for peptide bonds. Hydrogen bonds are formed by N(1)···O(2), 2.630(8) Å, and O1(W)···O2, 2.855 Å.

TABLE II. Selected bond lengths, angles, and torsions for compound **2**

Bond lengths (A1–A2)				Bond angles (A1–A2–A3)				Bond torsions (A1–A2–A3–A4)				
A1	A2	Type	Length, Å	A1	A2	A3	Angle, °	A1	A2	A3	A4	Torsion, °
C1	C2	Single	1.49(1)	C2	C1	O1	118.2(6)	O1	C1	C2	C3	177.8(6)
C1	O1	Delocalized	1.249(8)	O1	C1	O2	121.9(7)	C1	C2	C3	N1	–1.5(8)
C2	C3	Aromatic	1.421(7)	C2	C3	N1	117.7(5)	C2	C3	N1	C8	–176.5(6)
C3	N1	Single	1.410(7)	C3	N1	C8	129.8(5)	O3	C8	N1	C3	–1(1)
C8	N1	Single	1.332(7)	N1	C8	O3	127.4(6)	O3	C8	C8	O3	–180.0(6)
C8	O3	Double	1.23(1)									
C8	C8	Single	1.53(1)									

MTT Assay

The H_nobbz^{n-4} compounds were evaluated for their *in vitro* cytotoxic activity against a panel of human malignant and normal cell lines. Cytotoxic activity was evaluated using the standard MTT assay, after exposure of cells to the tested compounds for 48 h. The commercial antitumor agent doxorubicin (DOX) was used as a reference compound. HT29 and HeLa cells are particularly sensitive to **1**, evidenced by inhibited growth of the HT29 cell line, that is similar to the reference compound, and 2 times stronger cytotoxicity to HeLa. The results are given in Table III.

TABLE III. Cytotoxicity (IC_{50} / μM) of the ligand and complexes i*n vitro*

Compound	Cell line				
	MCF-7	A549	HT29	HeLa	MRC-5
Cisplatin	1.5	36.12	22.05	2.02	–
Doxorubicin (B)	0.75	7.86	0.32	1.17	0.12
H_4obbz (C)	>100	>100	**0.36**	**0.63**	>100
K_2H_2obbz (D)	>100	>100	>100	61.86	>100

*Effect of compound **1** on apoptosis in the HeLa cell line*

In order to explore how the modality of H_4obbz induced a decrease in the viability of HeLa cells, the nature of cell death was evaluated by the Annexin V/7-AAD staining assay. As H_4obbz (**1**) showed notable cytotoxicity towards the investigated cell lines, this compound was selected for further testing. HeLa cells were treated with IC_{50} concentrations of **1** or media alone (control) for 48 h. Flow cytometric analysis revealed that the primary mode of cell death in HeLa cells induced by **1** was apoptosis, with a negligible proportion of necrotic cells. Compound **1** significantly increased the proportion of apoptotic HeLa cells, the majority of them being early apoptotic, whereas necrotic cells, although in low percent, were noticeable only in the control cells (Fig. 2).

G_0/G_1 cell cycle arrest in HeLa cell line

To further reveal the mechanisms underlying the cytotoxic activity of **1** on cell cycle, the distribution of HeLa cells was determined by flow cytometry (Fig. 3).

A 48-h treatment with **1** almost completely arrested DNA synthesis as the S phase had nearly disappeared (0.6 %). The percentage of HeLa cells accumulated in the G0/G1 phase increased from 74.9 % (control) to 79.6 % when treated with **1**. HeLa cells show no changes in cell cycle profile of G2/M cells. The disappearance of the S phase and arrest at the G0/G1 phase, induced by **(1)**, points to the blockade of DNA synthesis as a possible mechanism that triggers apoptosis.

Apoptosis and cell cycle progression are connected. Cell cycle machinery has numerous regulatory molecules that monitor and regulate the advancement of the cell cycle. These regulatory molecules are activated after DNA damage, and

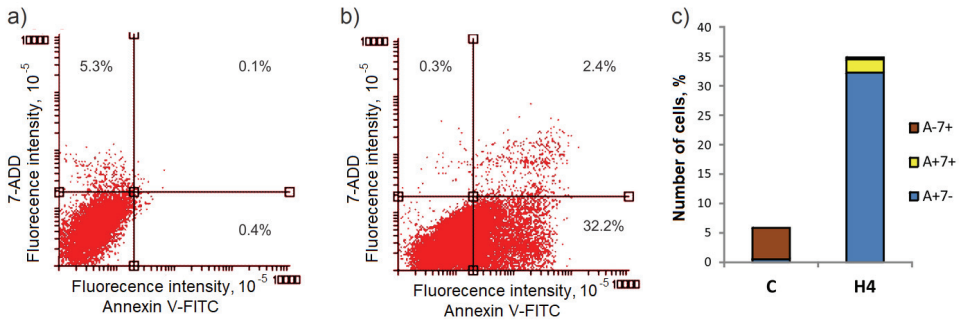

Fig. 2. Annexin V-FITC/7-AAD detection of apoptosis by flow cytometry. Dot plots illustrate distribution of viable, early apoptotic, late apoptotic and necrotic HeLa cells in untreated control (C) and treated with H_4obbz (H4). Lower left quadrant corresponds to viable cells (A– 7–), lower right to early apoptotic (A+ 7–), upper right to late apoptotic (A+ 7+) and upper left to necrotic cells (A– 7+). a) Control; b) H_4obbz; c) percentage of apoptotic and necrotic cells.

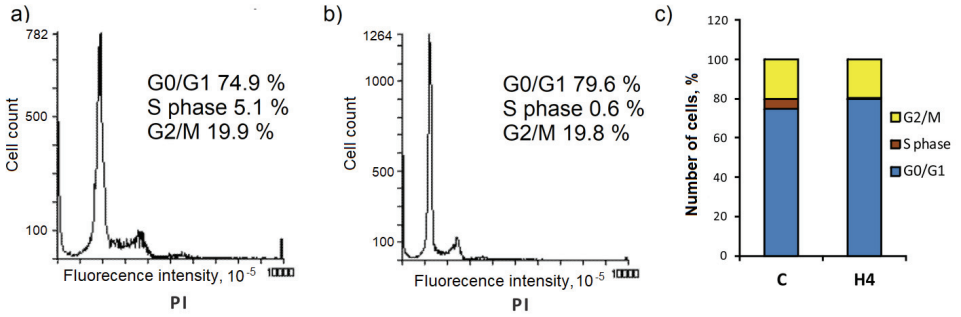

Fig. 3. Cell cycle analysis. a) Control; b) H_4obbz; c) the histograms demonstrate the cell cycle distribution of untreated HeLa cells in control sample (C) and cells treated with H_4obbz (H4).

they inhibit cell cycle progression allowing the cell to recover and repair the defect. If the damage cannot be fixed, programmed cell death launches and the cell is eliminated by apoptosis. On the other hand, genes that are supervising apoptosis are also implicated in the progression of the cell cycle. Either antiapoptotic (Bcl-2) or proapoptotic (Bax) regulatory proteins, aside from controlling the life and death of the cell, can inhibit cell cycle progression. Both molecules are transcriptional targets for p53, a tumor suppressor protein that either induces cell cycle arrest or apoptosis. Coordinated action of these molecules is pivotal for controlling cell fate.[32]

Apoptosis and cell cycle progression are connected. Cell cycle machinery has numerous regulatory molecules that monitor and regulate the advancement of the cell cycle. These regulatory molecules are activated after DNA damage, and they inhibit cell cycle progression, allowing the cell to recover and repair the defect. If the damage cannot be fixed, programmed cell death launches and the

cell is eliminated by apoptosis. On the other hand, genes that are supervising apoptosis are also implicated in the cell cycle progression. Either antiapoptotic (Bcl-2) or proapoptotic (Bax) regulatory proteins, besides controlling the life and death of the cell, can inhibit cell cycle progression. Both molecules are transcriptional targets for p53, a tumor suppressor protein that either induces cell cycle arrest or apoptosis. Coordinated action of these molecules is pivotal for controlling cell fate.[32]

Western blot (WB)

WB analysis of the effects of doxorubicin and **1** (Fig. 4) indicates that these compounds slightly modulate the total amount of the Bcl-2 protein compared to the control. When treated with **1**, in comparison with doxorubicin, the expression of Bcl-2 was lower, the expression of Bax was higher, and the expression of caspase-3 was slightly higher. Western blot analysis also demonstrated comparable but relatively low proteolytic cleavage of PARP in HeLa cells following treatment with the tested substances. The majority of chemotherapeutics induce apoptosis that is characterized by a significant expression of the Bax protein although, it was confirmed that apoptosis in various human solid tumors can be induced in the absence of any change in the level of the Bax protein.[33] In the present experiments, the analyzed compounds did not show high influence on the expression of the Bax protein. Caspases, a family of aspartate-specific cysteine proteases, play a critical role in the programmed cell death.

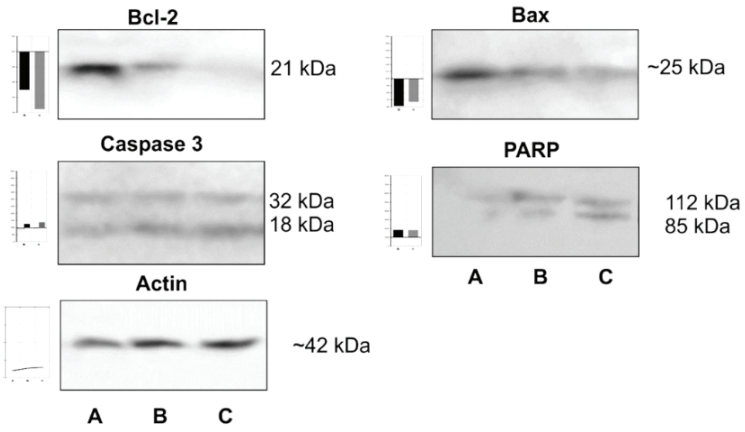

Fig. 4. Left: graphical presentation of densitometry data of protein expression obtained by Western blot analysis and processed with the ImageJ image computer program. A – control; B – doxorubicin; C – H_4obbz; right: the expression of apoptotic proteins investigated by Western blot analysis.

Caspases are important mediators in the initiation and execution of apoptotic signals.[3] The morphology of an apoptotic cell may be induced not only by cas-

pase activity, but also by the action of other families of proteases. Antitumor agents may induce cell death by apoptosis in a caspase-dependent or caspase--independent manner.[33,34] This means that apoptosis can be initiated without caspase activation, and caspase activation does not always result in cell death.[35] Doxorubicin and **1** both inhibit the growth of HeLa cells, and the degree of inhibition depends on the concentration of the test substance. The response type for the tested compounds were the same for all tested times. It was found that H_4obbz (**1**) shows a high antiproliferative effect (Table III).

It was proposed in a very recent work[2] that ER stress could be the mechanism that explains the action of the candidate drug. However, beside very probable L-protein (ER Chaperons) adduct, the possibility that the candidates interact with DNA could not be excluded. WB finding of Bcl2 expression and cleavage of PARP are in accordance with the present assumption. Roseti *et al*. showed that a novel ER stress-triggered caspase cascade, initiated by caspase-4 and involving caspase-8 and caspase-3, plays an important role in spontaneous B-cl2 cell apoptosis.[36] They also claim that ER stress triggers survival signals in B-cl2 cells by increasing GRP78 expression show that ER triggers an essential pathway for apoptosis of B-cl2 cell, and suggest that genetic and pharmacologic manipulation of ER signaling could represent an important therapeutic strategy. We do believe that the present compound fits well with the above findings and further support an ER stress mechanism as a real option with computational methods.

Docking

The structure of the target protein was downloaded directly from the RSCB PDB site (PDB entry 3LDL) and prepared as described in the Supplementary material. Co-crystalized ATP molecule was used to validate the docking method. Partial charges for all the docked structures were derived from B3LYP/TZVP QM calculations. The results of docking with both AD4 and Vina are presented in Table IV. Both programs managed to replicate the modes of binding of co--crystalized ATP. The structures of obtained results, overlaid with the crystal structure, are shown in Fig. S-1. Vina replicated crystal structure with objectively higher success.

TABLE IV. Binding energies derived from different docking software; E – estimated free energy of binding, K_i – estimated inhibition constant

Compound	AD4		Vina
	E / kJ mol^{-1}	K_i / μM	E / kJ mol^{-1}
ATP	–33.89	1.16	–47.28
H_2obbz^{2-}	–32.30	2.18	–41.84
H_4obbz	–30.17	5.22	–40.17

The binding location was defined using ATP groups as references. Phosphate groups interact with LYS296 and backbone amide nitrogens of THR37, THR38 and TYR39; Hydroxy groups of ribose interact with GLU293 and LYS296; aromatic rings of adenine interact *via* π-electrons with ARG297 and ARG367. Among others, these crucial interactions are pictured in Fig. 5.

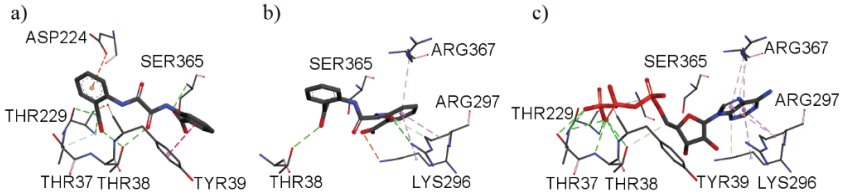

Fig. 5. Crucial actualized interactions of docking results towards Grp78: a) H_2obbz^{2-}, best score from Vina; b) H_2obbz^{2-}, best score from AD4; c) ATP, best score from Vina.

Relative energies obtained from the docking of H_2obbz^{2-} and H_4obbz in different programs agree, both slightly favoring the ionized form. AD4 and Vina seem to favor different binding modes, but both programs give almost identical solutions for the ionized and neutral form. AD4 tends to favor interactions of aromatic π-electrons of a benzoic acid moiety with ARG297 and ARG367. Instead, Vina tends to favor interactions of the carboxyl group of the benzoic acid moiety with backbone amide nitrogen of THR37 and THR38. Tested molecules are not large enough to reach both points of interest. Since both programs give solutions that interact with SER365, this residue can be considered the central point of interest. Each identified binding mode can be responsible for deactivation of Grp78 since hydrolysis of ATP at this site is crucial for the function of the protein.

Molecular dynamics

The efficacy of obbz ligands is restricted by the ability to interact with cell components. Therefore, the possible studies on the mechanism of the ligands reflected in their interaction with the either DNA or cell proteins responsible for the normal function of the cell. As mentioned above and in earlier papers the ER and cytosolic stress mechanisms as the results of docking to chaperons Grp78 and Hsc70 are predictive for more potent inhibitors, such as obbz compounds (Fig. 6).

Recent studies show that some ligands with O-donor atoms can be expected to induce ER stress and nucleus-independent apoptotic signaling. Wang *et al.*[37] were led to the conclusion that overexpression of CHOP proteins induced by the N,O ligands leads to apoptosis the cancer cell. However, Macias *et al.*[19] stated that Grp78 overexpression in tumor cells appears necessary to survive oncogenic stress. Elevated glucose metabolism leads to glucose starvation, low pH, and severe hypoxia, which are conditions under which cancer cells must survive, and are all factors that induce ER stress and activation of the Grp78 promoter. Hence,

according to these authors, successful inhibition of Grp78 from ER or cytosolic HSP70 heat shock proteins may alter the cancer cell survey.

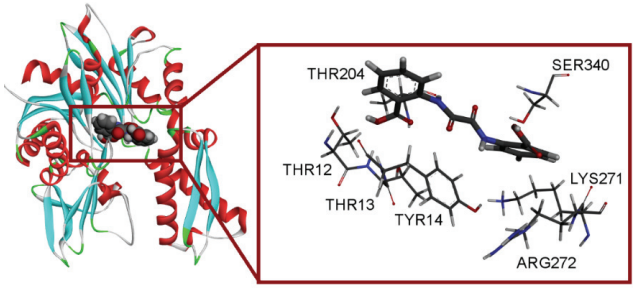

Fig. 6. MD system consisting of Grp78 monomer and the H_4obbz ligand.

Thus, it was decided to investigate the dynamics between the ligands (H_4obbz, H_2obbz^{2-} and ATP^{4-} found in 3LDL structure) and apo-Grp78 monomer, to determine how powerfully the Grp78 binds these agents comparing [L]-Grp78 free binding energies. RMSD plots of heavy atoms of the ligands and backbone N, CA, and C atoms in the Grp78 monomer along 5 trajectories (for each complex there are 5 independent samplings) are shown in Fig. 7. Usually, it is consider that small *RMSD* values along the trajectory indicate a stable state of the molecular system. Generally it can be seen see that the *RMSD* values of complexes are small (≈0.5 Å) with some exceptions due to the conformational change of the ligand. Similarly, the *RMSD* of the whole system have average values of 2 Å (Fig. 7); Some sudden jumps between small and large *RMSD* values of the protein backbone atoms are due to a periodic boundary issue.

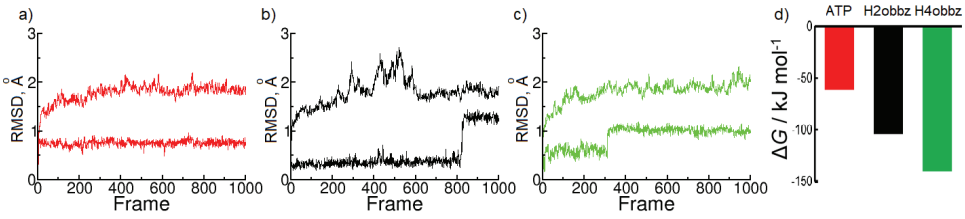

Fig. 7. *RMSD* values during MD simulation runs of Grp78 with: a) ATP; b) H_2obbz^{2-}; c) H_4obbz; higher values of *RMSD* are for protein-ligand complex while lower values are calculated only for atoms belonging to ligand; d) relative Δ*G* binding energies.

It was found that the ligands remained bound to the protein. The average distance between the center of the ligands and the surroundings residues at the binding pocket remain less than 8 Å (LYS271, THR12, THR13 and TYR14; GLU268 and LYS271; ARG272, ARG347 and SER275 – residue numeration differs by –25 from original PDB due to renumbering by Amber). In all trajectories, the

ligands were kept bound to the protein during the simulation runs. A further investigation[22] suggests that MMGBSA results serve better when used for comparison between similar molecules bonded at the same protein pocket. The results of MMGBSA analyses are in accordance with the expectations ΔG: –139.9992, –104.0201 and –61.1207 kJ mol^{-1} for H_4obbz, H_2obbz^{2-} and ATP, respectively (shown in Fig. 7 and given in Table S-I). Domain movement during the MD simulations was investigated using the online tool DynDom.[38] No domain movements during each of the simulations were found. Interactions of ligands with the most important residues in Grp78 are shown in the 2D diagram in Fig. S-3. After a thorough inspection of all trajectories in case of each [L]-Grp78 unit, i the following should be pointed out: a) The [L]-Grp78 unit behaves similarly and shows no tendency for separation from protein or their movement from the binding pocket; b) the oxamide (**1**) interacts with the THR13, TYR14 and GLY339 residues by strong hydrogen bonds and GLY339 and ARG271 residues by π-stacked and π-alkyl attraction; c) the secondary structure of the protein units were almost conserved; d) there were no domain movements of investigated protein during any of the simulations.

CONCLUSIONS

In this work 2,2'-[(1,2-dioxoethane-1,2-diyl)diimino]dibenzoic acid, H_4obbz (**1**) and its K^+ salt K_2H_2obbz (**2**) were synthetized and characterized by the spectroscopic and structural methods. The crystal structure of **2** was determined by X-ray analysis. Compound **2** crystallizes as a dipotassium salt of **1**. Compound **1** inhibited the growth of HeLa cell line similarly to the reference compound and expressed 4 times stronger cytotoxicity to HT29. Additionally, **1** exerted no toxic effects towards the healthy line (>100 μM). Flow cytometric analysis revealed that the primary mode of cell death in HeLa cells, induced by **1** was apoptosis, with a negligible proportion of necrotic cells. Treatment with **1** almost completely arrested DNA synthesis as the S phase had nearly disappeared. Western Blot and computational experiments further support the ER stress mechanism as a real option. Both docking and MD are indicative for tight binding between H_4obbz and the Grp78 chaperon. Vina and AD4 favor different binding modes in the active spot but both give comparable relative energies. Concerning MD simulations, the compounds were kept bound to the protein during the NPT production run. There were no domain movements of the investigated protein during any of the simulations. The results of MMGBSA analyses were in accordance with expectation ΔG: –139.9992, –104.0201 and –61.1207 kJ mol^{-1} for H_4obbz, H_2obbz^{2-} and ATP, respectively.

Acknowledgement. This work was supported by the Ministry of Education, Science and Technological Development of Serbia (Agreement No. 451-03-9/2021-14/200122).

ИЗВОД

СТРУКТУРНА, БИОЛОШКА И РАЧУНСКА ИПИТИВАЊА ДЕРИВАТА ОКСАМИДА

ИГЊАТ П. ФИЛИПОВИЋ[1], ЕМИНА М. МРКАЛИЋ[2], GIORGIO PELOSI[3], ВЕСНА КОЈИЋ[4], ДМИТАР ЈАКИМОВ[4], ДЕЈАН БАСКИЋ[5] и ЗОРАН Д. МАТОВИЋ[1]

[1]Универзитет у Крагујевцу, Природно–математички факултет, Институт за хемију, 34000 Крагујевац, [2]Универзитет у Крагујевцу, Институт за информационе технологије Крагујевац, 34000 Крагујевац, [3]Department of Chemistry, Life Sciences and Environmental Sustainability, University of Parma, 43123 Parma, Italy, [4]Институт за онкологију Војводине, Сремска Каменица, Нови Сад, Индустријски пут 4, 21204, Сремска Каменица и [5]Универзитет у Крагујевцу, Факултет медицинских наука, 34000 Крагујевац

Једињење 2,2'-[(1,2-диоксоетан-1,2-диил)диимино]дибензоева киселина (1, H_4obbz), и дикалијумова со овог једињења (**2**, K_2H_2obbz) су синтетисана и окарактерисана. Кристална структура једињења **2** је утврђена помоћу дифракције рендгенских зрака. Утврђена је цитотоксична активност према четири различита типа малигних ћелијских линија (MCF-7, A549, HT-29, HeLa), и према једној здравој ћелијској линији (MRC-5). Резултати указују разумну цитотоксичност која зависи од дозе, код једињења која показују селективност према малигним ћелијама у односу на здраве. Проточном цитометријом и флуоросцентном микроскопијом показано је да H_4obbz доводи до апоптозе и заустављања G0/G1 ћелијског циклуса, што указује на блокаду ДНК синтезе као могућ механизам дејства. Симулације молекулског доковања и молекулске динамике дају сличне одговоре на питање интеракција нашег једињења са хапероном Grp78. Слободне енергије везивања одређене MMGBS методом су у распону од –104 до –140 kJ mol^{-1}.

(Примљено 4. децембра, ревидирано 28 децембра, прихваћено 29. децембра 2021)

REFERENCES

1. Z. D. Matović, E. Mrkalić, G. Bogdanović, V. Kojić, A. Meetsma, R. Jelić, *J. Inorg. Biochem.* **121** (2013) 134 (https://doi.org/10.1016/j.jinorgbio.2013.01.006)
2. E. M. Mrkalić, R. M. Jelić, O. R. Klisurić, Z. D. Matović, *J. Chem. Soc. Dalt. Trans.* **43** (2014) 15126 (https://doi.org/10.1039/c3dt53384k)
3. S. Kumar, *Cell Death Differ.* **14** (2007) 32 (https://doi.org/10.1038/sj.cdd.4402060)
4. C. M. Palermo, C. A. Bennett, A. C. Winters, C. S. Hemenway, *Leuk. Res.* **32** (2008) 633 (https://doi.org/10.1016/j.leukres.2007.08.002)
5. C. Assunção Guimarães, R. Linden, *Eur. J. Biochem.* **271** (2004) 1638 (https://doi.org/10.1111/j.1432-1033.2004.04084.x)
6. L. Galluzzi, O. Kepp, G. Kroemer, *Oncogene* **31** (2012) 2805 (https://doi.org/10.1038/onc.2011.459)
7. Y. Qiao, C. Dsouza, A. A. Matthews, Y. Jin, W. He, J. Bao, F. Jiang, R. Chandna, R. Ge, L. Fu, *Eur. J. Med. Chem.* **193** (2020) 112228 (https://doi.org/10.1016/j.ejmech.2020.112228)
8. K. Nakatani, J. Y. Carriat, Y. Journaux, O. Kahn, F. Lloret, J. P. Renard, Y. Pei, J. Sletten, M. Verdaguer, *J. Am. Chem. Soc.* **111** (1989) 5739 (https://doi.org/10.1021/ja00197a036)
9. G.M. Sheldrick, *SADABS, Siemens Area Detector Absorption Correction Software*, University of Göttingen, Göttingen, 1996
10. G.M. Sheldrick, *SHELXL97, Program for Structure Refinement*, University of Göttingen, Göttingen, 1997

11. L. J. Farrugia, *J. Appl. Crystallogr.* **32** (1999) 837 (https://doi.org/10.1107/S0021889899006020)
12. W. Schmitz, *Krist. Und Tech.* **10** (1975) K120 (https://doi.org/10.1002/crat.19750101116)
13. M. N. Burnett, C. K. Johnson, *ORTEP-III: Oak Ridge Thermal Ellipsoid Plot Program for crystal structure illustrations*, Oak Ridge, TN, 1996 (https://doi.org/10.2172/369685)
14. *Gaussian 09, Revision A.02,* Gaussian, Inc., Wallingford CT, 2016
15. A. D. Becke, *Phys. Rev., A* **38** (1988) 3098 (https://doi.org/10.1103/PhysRevA.38.3098)
16. C. Lee, W. Yang, R. G. Parr, *Phys. Rev. B* **37** (1988) 785 (https://doi.org/10.1103/PhysRevB.37.785)
17. A. D. Becke, *J. Chem. Phys.* **98** (1993) 5648 (https://doi.org/10.1063/1.464913)
18. M. F. Peintinger, D. V. Oliveira, T. Bredow, *J. Comput. Chem.* **34** (2013) 451 (https://doi.org/10.1002/jcc.23153)
19. A. T. Macias, D. S. Williamson, N. Allen, J. Borgognoni, A. Clay, Z. Daniels, P. Dokurno, M. J. Drysdale, G. L. Francis, C. J. Graham, R. Howes, N. Matassova, J. B. Murray, R. Parsons, T. Shaw, A. E. Surgenor, L. Terry, Y. Wang, M. Wood, A. J. Massey, *J. Med. Chem.* **54** (2011) 4034 (https://doi.org/10.1021/jm101625x)
20. G. Jones, P. Willett, R. C. Glen, A. R. Leach, R. Taylor, *J. Mol. Biol.* **267** (1997) 727 (https://doi.org/10.1006/jmbi.1996.0897)
21. O. Trott, A. J. Olson, *J. Comput. Chem.* **31** (2010) 455 (https://doi.org/10.1002/jcc.21334)
22. *Amber 2021*, University of California, San Francisco, CA, 2021
23. W. L. Jorgensen, J. Chandrasekhar, J. D. Madura, R. W. Impey, M. L. Klein, *J. Chem. Phys.* **79** (1983) 926 (https://doi.org/10.1063/1.445869)
24. W. L. Jorgensen, J. D. Madura, *Mol. Phys.* **56** (1985) 1381 (https://doi.org/10.1080/00268978500103111)
25. P. Li, L. F. Song, K. M. Merz, *J. Chem. Theory Comput.* **11** (2015) 1645 (https://doi.org/10.1021/ct500918t)
26. A. W. Götz, M. J. Williamson, D. Xu, D. Poole, S. Le Grand, R. C. Walker, *J. Chem. Theory Comput.* **8** (2012) 1542 (https://doi.org/10.1021/ct200909j)
27. R. Salomon-Ferrer, A. W. Götz, D. Poole, S. Le Grand, R. C. Walker, *J. Chem. Theory Comput.* **9** (2013) 3878 (https://doi.org/10.1021/ct400314y)
28. S. Le Grand, A. W. Götz, R. C. Walker, *Comput. Phys. Commun.* **184** (2013) 374 (https://doi.org/10.1016/j.cpc.2012.09.022)
29. M. S. Jeremić, H. Wadepohl, V. V. Kojić, D. S. Jakimov, R. Jelić, S. Popović, Z. D. Matović, P. Comba, *RSC Adv.* **7** (2017) 5282 (https://doi.org/10.1039/C6RA26199J)
30. T. Mosmann, *J. Immunol. Methods* **65** (1983) 55 (https://doi.org/10.1016/0022-1759(83)90303-4)
31. N. Khanna, H. Jayaram, N. Singh, *Life Sci.* **75** (2004) 179 (https://doi.org/10.1016/j.lfs.2003.11.026)
32. S. Zinkel, A. Gross, E. Yang, *Cell Death Differ.* **13** (2006) 1351 (https://doi.org/10.1038/sj.cdd.4401987)
33. R. Kim, M. Emi, K. Tanabe, Y. Uchida, K. Arihiro, *Eur. J. Surg. Oncol.* **32** (2006) 269 (https://doi.org/10.1016/j.ejso.2005.12.006)
34. G. Kroemer, S. J. Martin, *Nat. Med.* **11** (2005) 725 (https://doi.org/10.1038/nm1263)
35. J. Peng, X. Chen, Q. Hu, M. Yang, H. Liu, W. Wei, S. Liu, H. Wang, *Mol. Med. Rep.* **10** (2014) 2271 (https://doi.org/10.3892/mmr.2014.2489)

36. E. Rosati, R. Sabatini, G. Rampino, F. De Falco, M. Di Ianni, F. Falzetti, K. Fettucciari, A. Bartoli, I. Screpanti, P. Marconi, *Blood* **116** (2010) 2713 (https://doi.org/10.1182/blood-2010-03-275628)
37. Y. Wang, J. Hu, Y. Cai, S. Xu, B. Weng, K. Peng, X. Wei, T. Wei, H. Zhou, X. Li, and Guang Liang, *J. Med. Chem* **56** (2013) 9601 (https://doi.org/10.1021/jm4016312)
38. C. Girdlestone, S. Hayward, *J. Comput. Biol.* **23** (2016) 21 (https://doi.org/10.1089/cmb.2015.0143).